Exceptional Contours and Band Structure Design in Parity-Time Symmetric Photonic Crystals

Alexander Cerjan, Aaswath Raman, and Shanhui Fan

Phys. Rev. Lett. **116**, 203902 — Published 20 May 2016

DOI: 10.1103/PhysRevLett.116.203902

Exceptional contours and band structure design in parity-time symmetric photonic crystals

Alexander Cerjan, Aaswath Raman, and Shanhui Fan*
Department of Electrical Engineering, and Ginzton Laboratory, Stanford University, Stanford, California 94305, USA
(Dated: March 28, 2016)

We investigate the properties of two-dimensional parity-time symmetric periodic systems whose non-Hermitian periodicity is an integer multiple of the underlying Hermitian system's periodicity. This creates a natural set of degeneracies which can undergo thresholdless $\mathcal{PT}$ transitions. We derive a $\mathbf{k} \cdot \mathbf{p}$ perturbation theory suited to the continuous eigenvalues of such systems in terms of the modes of the underlying Hermitian system. In photonic crystals, such thresholdless $\mathcal{PT}$ transitions are shown to yield significant control over the band structure of the system, and can result in all-angle supercollimation, a $\mathcal{PT}$-superprism effect, and unidirectional behavior.

There has been significant recent interest in the properties of parity-time symmetric systems, which are invariant under the combined action of parity ($\mathcal{P}$) and time reversal ($\mathcal{T}$) operations. Such systems were initially explored due to their connection to the theoretical foundations of quantum mechanics [1, 2]. Subsequently, $\mathcal{PT}$ symmetric optical systems have garnered attention as they enable novel capabilities for the control of light propagation [3–15].

In spite of substantial progress in this field, there remain significant challenges and opportunities. First, the vast majority of $\mathcal{PT}$ symmetric structures in optics have focused on either effective zero-dimensional systems, such as coupled cavity systems [16–20], or one-dimensional systems, such as waveguide arrays [21, 22], ring lasers [23], and one-dimensional lattice systems [24–26]. A few recent studies of specific multi-dimensional $\mathcal{PT}$ symmetric systems have demonstrated exotic properties not found in low-dimensional systems, such as band flattening and continuous rings of exceptional points [4, 27–29]. Yet despite these promising initial results, a systematic exploration of higher dimensional $\mathcal{PT}$ symmetric systems has not been previously reported. Second, thresholdless $\mathcal{PT}$ transitions have been recently discovered, for which the $\mathcal{PT}$ symmetry is spontaneously broken in the presence of an infinitesimal amount of gain and loss [30]. Realizing thresholdless $\mathcal{PT}$ symmetry transitions is of interest as they reduce the experimental requirements for observing exceptional point physics. However, there has not been a systematic approach for achieving thresholdless $\mathcal{PT}$ symmetry transitions, especially in higher dimensional systems. In previous works, one typically acquires a thresholdless PT symmetry transition from point degeneracies, either accidental [29], or from lattice symmetry such as the Dirac point that arise in a honeycomb lattice [27, 28]. However, such point degeneracies require careful engineering of the crystal geometry, and are restricted to forming rings of exceptional points at the $\mathcal{PT}$ transition boundary.

In this Letter, we provide a systematic study of higher-dimensional $\mathcal{PT}$ symmetric photonic crystals, and introduce a general mechanism for realizing thresholdless $\mathcal{PT}$ transitions. We consider two-dimensional $\mathcal{PT}$ symmetric photonic crystals (PhC), whose non-Hermitian primitive cell is an integer multiple of the primitive cell of the underlying Hermitian system. We show that under a very general set of conditions, such systems always exhibit a thresholdless $\mathcal{PT}$ transition in part of the wavevector space. Moreover, such a system enables a new form of band structure engineering, and can result in a $\mathcal{PT}$-superprism effect, unidirectional behavior, and all-angle supercollimation, which are distinct from related effects in Hermitian PhCs [31–35], and not all of which are present in previous thresholdless transition schemes. Furthermore, our mechanism is readily generalizable to more complex two-dimensional systems, such as coupled cavity waveguides [36, 37], and three-dimensional systems.

To illuminate this process, as an example, we consider the two-dimensional PhC formed of dielectric square rods with alternating gain or loss of equal magnitude embedded in air depicted in Fig. 1(a). The primitive cell of this structure contains two square rods, one containing gain and a neighbor containing loss. In the absence of gain and loss, the underlying Hermitian system, shown in Fig. 1(b), has a smaller primitive cell containing a single dielectric rod. For semantic convenience, we will henceforth refer to this larger primitive cell as the 'supercell,' and reserve 'primitive cell' for the underlying Hermitian system.

The band structure of the underlying Hermitian system, plotted with respect to the supercell, is shown in Fig. 1(c) and 1(d) for the first and third sets of TM bands. We see that the band structure is folded along the $k_x = \pi/2a$ line, where a is the primitive cell lattice spacing, creating a degenerate contour. As gain and loss are added to the system, these degenerate contours experience thresholdless $\mathcal{PT}$ transitions immediately, while neighboring locations in wavevector space undergo ordinary $\mathcal{PT}$ transitions, as can be seen in Figs. 1(e)-1(h). This causes the folded bands to merge together outwards from the degenerate contour, forming the requisite complex conjugate pairs of frequencies, while the boundary

between the merged and independent regions is a contour comprised entirely of exceptional points. In the wake of this folding process, the bands nearly flatten in the x-direction perpendicular to the degenerate contour. The total proportion of merged wavevector space as a function of τ is shown in Fig. S1 in the supplementary material [38].

We now show that the behavior as observed above is generally present in $\mathcal{PT}$ symmetric PhCs that have an enlarged primitive cell (i.e. a 'supercell') as compared to the underlying Hermitian system (i.e. a 'primitive cell'). The band structure of a $\mathcal{PT}$ symmetric PhC is defined by

$$\left[\nabla\times\nabla\times-\left(\varepsilon(\mathbf{x})+i\tau g(\mathbf{x})\right)\frac{\omega_n^2(\mathbf{k})}{c^2}\right]\mathbf{E}_{n\mathbf{k}}(\mathbf{x})=0, \quad (1)$$

in which $\mathbf{E}_{n\mathbf{k}}(\mathbf{x})$ is the mode profile of the nth band with wavevector $\mathbf{k}$ and frequency $\omega_n(\mathbf{k})$, $\varepsilon(\mathbf{x})$ is the Hermitian dielectric function of the PhC, and τ and $g(\mathbf{x})$ are the strength and distribution of the gain and loss in the PhC respectively. We assume that the primitive cell has a set of lattice vectors $\{\mathbf{a}\}$ such that $\varepsilon(\mathbf{x}+\mathbf{a}_i)=\varepsilon(\mathbf{x})$, while the supercell has lattice vectors $\{\mathbf{A}\}$, which are usually integer multiples of the primitive cell lattice vectors, $\mathbf{A}_i=\sum_j n_{ij}\mathbf{a}_j$, such that $g(\mathbf{x}+\mathbf{A}_i)=g(\mathbf{x})$. We also define the supercell's reciprocal lattice vectors $\mathbf{B}_i$, such that $\mathbf{B}_i\cdot\mathbf{A}_j=2\pi\delta_{ij}$. Given the periodicity of the supercell, the mode profiles obey the supercell translation symmetry,

$$\mathbf{E}_{n\mathbf{k}}(\mathbf{x}+\mathbf{A}_j)=e^{i\mathbf{k}\cdot\mathbf{A}_j}\mathbf{E}_{n\mathbf{k}}(\mathbf{x}). \quad (2)$$

Finally, the gain and loss are applied such that $g(\mathbf{x})=-g(-\mathbf{x})$, and we adopt the convention that $\tau\geq 0$.

Our objective is to explore the behavior of the band structure in the vicinity of a particular set of $\mathbf{k}$-points such as the degenerate contour. Thus, for a region of $\mathbf{k}$-space in the neighborhood of a wavevector $\mathbf{k}_0$, we expand the supercell wavefunctions at $\mathbf{k}$ in terms of those at $\mathbf{k}_0$ as

$$\mathbf{E}_{n\mathbf{k}}(\mathbf{x})=\sum_m C_{nm}(\mathbf{k})e^{i(\mathbf{k}-\mathbf{k}_0)\cdot\mathbf{x}}\mathbf{E}^{(0)}_{m\mathbf{k}_0}(\mathbf{x}), \quad (3)$$

where $\mathbf{E}^{(0)}_{m\mathbf{k}}(\mathbf{x})$ satisfies Eq. (1) with $\tau=0$, and C_{nm} are the complex expansion coefficients [39, 40]. In doing so, we avoid the difficulties associated with using the Bloch modes of a non-Hermitian structure [4, 6, 8], and can normalize the wavefunctions in the usual manner,

$$\int_{\mathrm{SC}}\varepsilon(\mathbf{x})\left(\mathbf{E}^{(0)}_{n\mathbf{k}}(\mathbf{x})\right)^*\cdot\mathbf{E}^{(0)}_{m\mathbf{k}'}(\mathbf{x})d\mathbf{x}=\delta_{nm}\delta(\mathbf{k}-\mathbf{k}'), \quad (4)$$

where the integral is evaluated over the supercell. Furthermore, since the supercell with $\tau=0$ is an exact N-fold copy of the primitive cell, there are exactly N reciprocal lattice vectors that are integer multiples of the

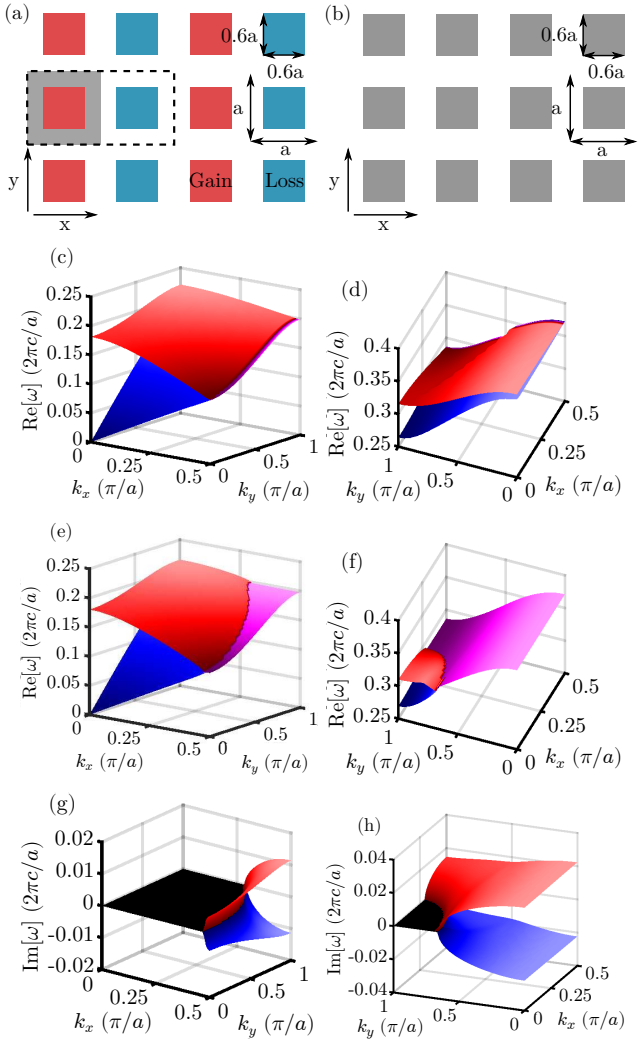

FIG. 1. (Color online) (a) Schematic of the 2D PhC comprised of square rods with side length $0.6a$ of dielectric, $\varepsilon_{die}=12$, embedded in air, $\varepsilon_{air}=1$, with a square primitive cell side length of a. The primitive cell is indicated in gray, while the supercell contains two primitive cells and is marked with a dashed border. When $\tau\neq 0$, the red rods contain gain, while the cyan rods contain loss. (b) Schematic of the underlying 2D Hermitian PhC. (c,e) Real part of the frequencies for the first (blue) and second (red) supercell TM bands when $\tau=0$ and $\tau=1.5$. Locations where the bands have merged are shown in magenta. (d,f) Real part of the frequencies for the fifth (blue) and sixth (red) supercell TM bands when $\tau=0$ and $\tau=1.5$. (g) Imaginary part of the frequencies for the first (blue) and second (red) supercell TM bands when $\tau=1.5$. Black denotes no imaginary component. (h) Imaginary part of the frequencies for the fifth (blue) and sixth (red) supercell TM bands when $\tau=1.5$.

members of $\{\mathbf{B}\}$ which generate the primitive Brillouin zone from the supercell Brillouin zone, and are denoted as $\mathbf{L}_1,...,\mathbf{L}_N$, such that $\mathbf{L}_j=\sum_i m_i\mathbf{B}_i$. Thus, as the translational symmetry of the underlying Hermitian system is described by the primitive cell, the states $\mathbf{E}^{(0)}_{m\mathbf{k}}(\mathbf{x})$ satisfy a 'hidden' translational symmetry, and can be chosen

such that

$$\mathbf{E}^{(0)}_{m\mathbf{k}}(\mathbf{x}+\mathbf{a}_j) = e^{i(\mathbf{k}+\mathbf{L}_i)\cdot\mathbf{a}_j}\mathbf{E}^{(0)}_{m\mathbf{k}}(\mathbf{x}). \quad (5)$$

Here, each supercell band m only satisfies this relationship for a single element $\mathbf{L}_j$ [41]. Furthermore, each of the supercell bands which correspond to the same unfolded band from the primitive Brillouin zone satisfies Eq. (5) for a different $\mathbf{L}$.

Upon substituting Eq. (3) into Eq. (1), multiplying through by $(\mathbf{E}^{(0)}_{l\mathbf{k}_0}(\mathbf{x}))^*$, and integrating over the supercell, we find the matrix equation

$$\sum_m \Big[\left(\omega_n^2(\mathbf{k}) - (\omega_m^{(0)}(\mathbf{k}_0))^2\right)\frac{\delta_{lm}}{c^2} + i\tau\frac{\omega_n^2(\mathbf{k})}{c^2}G_{lm} + \mathbf{s}\cdot\mathbf{P}_{lm} - s^2 Q_{lm}\Big] C_{nm}(\mathbf{k}) = 0, \quad (6)$$

where $\mathbf{s} = \mathbf{k}-\mathbf{k}_0$ and $\omega_m^{(0)}(\mathbf{k}_0)$ is the frequency of the mth band of the supercell system when $\tau = 0$. For ease of the following analysis we have specialized to 2D TM bands, but a full vectorial treatment is straightforward [38]. The matrix element G_{lm} contains the effects of modal coupling through the gain and loss,

$$G_{lm} = \int_{\mathrm{SC}} g(\mathbf{x})\left(E^{(0)}_{l\mathbf{k}_0}(\mathbf{x})\right)^* E^{(0)}_{m\mathbf{k}_0}(\mathbf{x})d\mathbf{x}, \quad (7)$$

while the elements $\mathbf{P}_{lm}$ and Q_{lm} represent the frequency shifts due to displacements in $\mathbf{k}$-space for the Hermitian system,

$$\mathbf{P}_{lm} = 2i\int_{\mathrm{SC}} \left(E^{(0)}_{l\mathbf{k}_0}(\mathbf{x})\right)^* \nabla E^{(0)}_{m\mathbf{k}_0}(\mathbf{x})d\mathbf{x}, \quad (8)$$

$$Q_{lm} = \int_{\mathrm{SC}} \left(E^{(0)}_{l\mathbf{k}_0}(\mathbf{x})\right)^* E^{(0)}_{m\mathbf{k}_0}(\mathbf{x})d\mathbf{x}. \quad (9)$$

Note, the group velocity for each band is given by the corresponding diagonal element of $\mathbf{P}$ as $\nabla_{\mathbf{k}}\omega_m(\mathbf{k}_0) = -c^2\mathbf{P}_{mm}/2\omega_m(\mathbf{k}_0)$, which is true even for locations with degenerate frequencies due to the requirement that $\mathbf{E}^{(0)}_{m\mathbf{k}_0}(\mathbf{x})$ satisfy Eq. (5). Furthermore, the hidden translational symmetry of the wave functions of the Hermitian supercell system yields two important restrictions upon the coupling matrix elements. First, it can be shown that by breaking up the integrals over the supercell into the individual primitive cell constituents, $\mathbf{P}_{lm}$ and Q_{lm} are only non-zero if $\mathbf{E}^{(0)}_{l\mathbf{k}_0}(\mathbf{x})$ and $\mathbf{E}^{(0)}_{m\mathbf{k}_0}(\mathbf{x})$ obey Eq. (5) for the same $\mathbf{L}_j$ [38]. Second, the odd parity symmetry of $g(\mathbf{x})$ results in $G_{mm} = 0$. As the wave functions for any point in $\mathbf{k}$-space form a complete set, Eq. (6) is an exact restatement of Eq. (1) (although extra considerations are necessary for vectorial fields [42]).

The application of gain and loss to the Hermitian system couples pairs of bands in the supercell system which originate from the same unfolded band of the primitive Brillouin zone. Thus, we will assume that we can decouple any such pair of bands from the rest of the system, and rewrite Eq. (6) for the reduced two-band system as

$$\frac{\omega^2(\mathbf{k})}{c^2}\begin{bmatrix} 1 & i\tau G_{12} \\ i\tau G_{21} & 1 \end{bmatrix}\mathbf{C} = \Omega(\mathbf{s},\mathbf{k}_0)\mathbf{C}, \quad (10)$$

where $\Omega_{ij}(\mathbf{s},\mathbf{k}_0) = [(\omega_i^{(0)}(\mathbf{k}_0)/c)^2 - \mathbf{s}\cdot\mathbf{P}_{ii} + s^2 Q_{ii}]\delta_{ij}$. By setting $\mathbf{s} = 0$, the non-Hermitian PhC satisfies Eq. (10) over all of $\mathbf{k}$-space, and Eq. (10) correctly reduces to Eq. (3) of Ge and Stone for systems with isolated modes [30], except that Eq. (10) has been derived for systems with continuous bands.

However, in contrast to previous works [25, 30], we can now choose $\mathbf{k} \neq \mathbf{k}_0$ to understand the band merging process. To this end, we select $\mathbf{k}_0$ to be a degenerate point of the supercell Hermitian system with frequency $\omega^{(0)}(\mathbf{k}_0)$, and solve for the frequencies of the non-Hermitian system as

$$\frac{\omega^2}{c^2} = \frac{2\Omega_{11}\Omega_{22}}{\Omega_{11}+\Omega_{22} \pm \sqrt{(\Omega_{11}-\Omega_{22})^2 - 4\Omega_{11}\Omega_{22}\tau^2|G_{12}|^2}}. \quad (11)$$

As the two supercell bands originate from the same primitive band, the association of $\mathbf{P}_{ii}$ with the group velocity yields two related conclusions. First, along the degenerate contour, $\partial\omega_1^{(0)}(\mathbf{k}_0)/\partial k_\parallel = \partial\omega_2^{(0)}(\mathbf{k}_0)/\partial k_\parallel \equiv -c^2 P_\parallel/2\omega^{(0)}$, while perpendicular to the degenerate contour, $\partial\omega_2^{(0)}(\mathbf{k}_0)/\partial k_\perp = -\partial\omega_1^{(0)}(\mathbf{k}_0)/\partial k_\perp \equiv -c^2 P_\perp/2\omega^{(0)}$, as the unfolded band of the primitive cell is smooth. Thus, the threshold for $\mathcal{PT}$ symmetry breaking to second order in $\mathbf{s} = (s_\perp, s_\parallel)$ is

$$\tau_{\mathrm{TH}} \approx \left| \frac{s_\perp P_\perp\left(1 + \frac{c^2 s_\parallel P_\parallel}{(\omega^{(0)}(\mathbf{k}_0))^2}\right) + \frac{s^2}{2}(Q_{22}-Q_{11})}{|G_{12}|\left(\frac{\omega^{(0)}(\mathbf{k}_0)}{c}\right)^2} \right|. \quad (12)$$

To first order, τ_{TH} is seen to be strictly dependent upon the perpendicular displacement in wavevector space from the degenerate contour, in agreement with the band structures seen in Figs. 1(e) and 1(f). Furthermore, the second order corrections yield an increase in the threshold calculated about a particular $\mathbf{k}_0$ if $\mathbf{s}$ also contains a component parallel to the degenerate contour. Thus, the correct (minimum) $\mathcal{PT}$ threshold for any point $\mathbf{k}$ is calculated from the closest location on the degenerate contour, and is seen to be strictly dependent upon $s_\perp$, demonstrating that the coupled bands of the non-Hermitian system merge together directly outwards from the degenerate contour continuously.

The flattening of the bands as they merge can be understood by solving for the frequency at the exceptional point (using $\mathbf{s} = s_\perp$),

$$\omega_{\mathrm{TH}}(\mathbf{k}) \approx \omega^{(0)}(\mathbf{k}_0)\left(1 + \frac{c^2 s_\perp^2 (Q_{11}+Q_{22})}{4(\omega^{(0)}(\mathbf{k}_0))^2}\right), \quad (13)$$

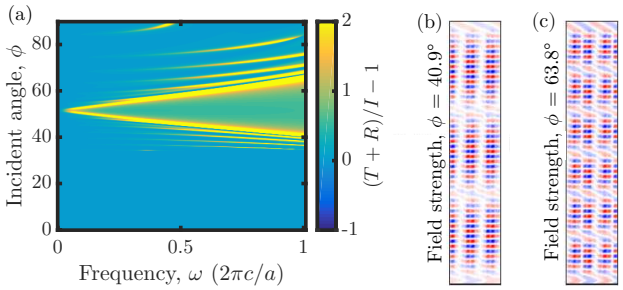

FIG. 2. (Color online) (a) Non-unitary behavior as a function of incident angle, ϕ, and $\mathcal{PT}$ symmetry breaking parameter, τ, for an s-polarized plane wave source with $\omega = 0.185(2\pi c/a)$ incident upon a PhC slab infinite in the x-direction and with 50 layers in the y-direction for the same system shown in Fig. 1(a). $\phi = 0$ corresponds to normal incidence in the y-direction. The PhC slab is surrounded by a passive dielectric with $\varepsilon = 3$. Values of 0 correspond to unitary behavior, while $[-1, 0)$ signifies absorption, and $(0, \infty]$ signifies amplification. The reflection and transmission coefficients were calculated using the Fourier Modal Method as implemented in S^4 [43]. (b-c) Plot of the real part of the electric field for the same structure with $\tau = 0.65$, and $\phi = 40.9°$ (b), or $\phi = 63.8°$ (c). Field plots were generated using the freely available MaxwellFDFD software package [44].

which is seen to be given by the associated degenerate frequency with the leading correction being second order in $(1/\omega^{(0)})$. As τ is increased beyond the threshold value for a particular location in wavevector space, the dominant change in the frequencies of the two bands is to acquire imaginary components, leaving the bands nearly flat after they merge.

The thresholdless $\mathcal{PT}$ transition of supercell $\mathcal{PT}$ symmetric PhCs can also be observed in the non-unitary behavior of related finite systems. Figure 2(a) shows the amplification and absorption as a function of incident angle and τ for a single frequency incident upon a PhC slab similar to Fig. 1(a), which is infinite in the x-direction, but finite in the y-direction. The frequency chosen lies within the range of frequencies comprising the degenerate contour of the first pair of bands, Fig. 1(e), and thus exhibits a thresholdless $\mathcal{PT}$ transition at a particular incidence angle. As τ is increased, the area of the $\mathcal{PT}$-broken region in $\mathbf{k}$-space is increased, resulting in a wider range of incident angles which yield amplification.

In Hermitian PhCs, the superprism effect refers to sharp features in the isofrequency contours of a band structure, where a small change in the incident angle of light yields an enormous change in the refraction angle of the light inside the PhC [31–33]. However, the exceptional contour of a $\mathcal{PT}$ PhC separates a region of non-Hermitian behavior from that of ordinary propagation. This yields a '$\mathcal{PT}$-superprism' effect, in which a small change in the incident angle of the signal results in either unitary or non-unitary behavior. For example, when $\tau = 0.65$, the system is unitary at $\phi = 39°$, and yet exhibits a tenfold increase in the net gain with the small

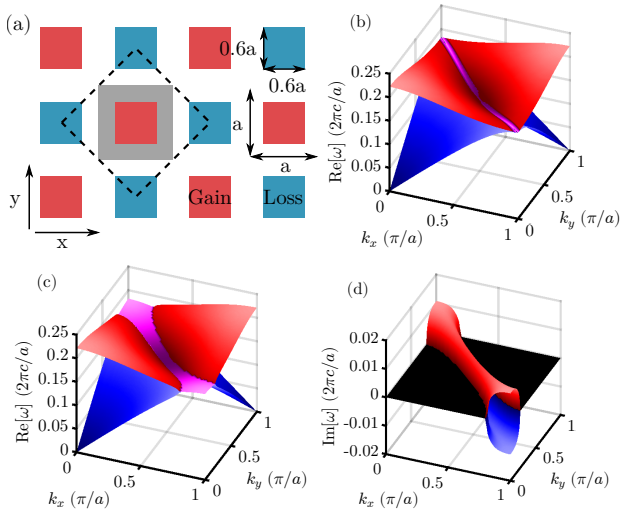

FIG. 3. (Color online) (a) Schematic of the 2D PhC comprised of square rods with side length $0.6a$ of dielectric, $\varepsilon_{die} = 12$, embedded in air, $\varepsilon_{air} = 1$, with a square primitive cell side length of a. The primitive cell is indicated in gray, while the supercell contains two primitive cells and is marked with a dashed border. When $\tau \neq 0$, the red rods contain gain, while the cyan rods contain loss. (b,c) Real part of the frequencies for the first (blue) and second (red) supercell TM bands when $\tau = 0$ and $\tau = 1.5$. Locations where the bands have merged are shown in magenta. (d) Imaginary part of the frequencies for the first (blue) and second (red) supercell TM bands when $\tau = 1.5$. Black denotes no imaginary component.

change of the incidence angle to $\phi = 44°$. This effect could have applications as an optical switch.

Likewise, flat features in isofrequency contours act as supercollimators, counteracting diffraction for incident beams with a finite width whose Fourier components lie within the flat contour [31, 34, 35]. As is seen in the band-merging process in Figs. 1(c)-1(h), by changing τ, flat contours can be designed with a desired width, potentially spanning the entire Brillouin zone, or removed entirely, allowing for tunable supercollimation or all-angle supercollimation for frequencies with completely merged bands. This phenomenon is in contrast to the circular isofrequency contours formed by $\mathcal{PT}$ systems stemming from isolated point degeneracies [27–29]. The effect of supercollimation can also be seen in the field profiles of the finite PhC system, where within the $\mathcal{PT}$-broken region the wavefunction propagates entirely in the y-direction, as can be seen in the field profiles at the edge of this region in Fig. 2(b) and 2(c). Finally, $\mathcal{PT}$ PhCs can exhibit unidirectional behavior [38].

By changing the distribution of gain and loss in the system while maintaining $\mathcal{PT}$ symmetry, we can change the location of the degenerate contour in $\mathbf{k}$-space. An example of this is shown in Fig. 3(a), where same underlying PhC from Fig. 1(b) is considered with a different application of gain and loss. The degenerate contour of the supercell Hermitian system now lies along the X-Y

contour of the primitive Brillouin zone, Fig. 3(b), and as τ is increased, the $\mathcal{PT}$-broken region is seen to expand away from this contour, Figs. 3(c) and 3(d). This enables a new form of band structure engineering, as both the initial choice and potential for electrical modulation of the degenerate contour result in qualitative changes to the optical properties of the PhC.

In conclusion, we have demonstrated that the degeneracies naturally generated in supercell $\mathcal{PT}$ symmetric PhCs can yield new control over band structure design. Experimentally, both the $\mathcal{PT}$-superprism effect and all-angle supercollimation can be observed in the analogous system with alternating elements of no-loss and double-loss, and thus should be observable in semiconductor based systems with embedded absorption [38].

We would like to thank Jessica Piper, Li Ge, and Steven G. Johnson for helpful discussions. This work was supported by the AFOSR MURI program (Grant No. FA9550-12-1-0471).

* shanhui@stanford.edu

[1] C. M. Bender, S. Boettcher, and P. N. Meisinger, J. Math. Phys. **40**, 2201 (1999).
[2] C. M. Bender, D. C. Brody, and H. F. Jones, Phys. Rev. Lett. **89**, 270401 (2002).
[3] Z. H. Musslimani, K. G. Makris, R. El-Ganainy, and D. N. Christodoulides, Phys. Rev. Lett. **100**, 030402 (2008).
[4] K. G. Makris, R. El-Ganainy, D. N. Christodoulides, and Z. H. Musslimani, Phys. Rev. Lett. **100**, 103904 (2008).
[5] S. Klaiman, U. Günther, and N. Moiseyev, Phys. Rev. Lett. **101**, 080402 (2008).
[6] S. Longhi, Phys. Rev. Lett. **103**, 123601 (2009).
[7] A. Guo, G. J. Salamo, D. Duchesne, R. Morandotti, M. Volatier-Ravat, V. Aimez, G. A. Siviloglou, and D. N. Christodoulides, Phys. Rev. Lett. **103**, 093902 (2009).
[8] K. G. Makris, R. El-Ganainy, D. N. Christodoulides, and Z. H. Musslimani, Phys. Rev. A **81**, 063807 (2010).
[9] C. E. Rüter, K. G. Makris, R. El-Ganainy, D. N. Christodoulides, M. Segev, and D. Kip, Nat. Phys. **6**, 192 (2010).
[10] Z. Lin, H. Ramezani, T. Eichelkraut, T. Kottos, H. Cao, and D. N. Christodoulides, Phys. Rev. Lett. **106**, 213901 (2011).
[11] Y. D. Chong, L. Ge, and A. D. Stone, Phys. Rev. Lett. **106**, 093902 (2011).
[12] M. Liertzer, L. Ge, A. Cerjan, A. D. Stone, H. E. Türeci, and S. Rotter, Phys. Rev. Lett. **108**, 173901 (2012).
[13] L. Ge, Y. D. Chong, and A. D. Stone, Phys. Rev. A **85**, 023802 (2012).
[14] V. Yannopapas, New J. Phys. **14**, 113017 (2012).
[15] V. Yannopapas, Phys. Rev. A **89**, 013808 (2014).
[16] B. Peng, Ş. K. Özdemir, F. Lei, F. Monifi, M. Gianfreda, G. L. Long, S. Fan, F. Nori, C. M. Bender, and L. Yang, Nat. Phys. **10**, 394 (2014).
[17] B. Peng, Ş. K. Özdemir, S. Rotter, H. Yilmaz, M. Liertzer, F. Monifi, C. M. Bender, F. Nori, and L. Yang, Science **346**, 328 (2014).
[18] L. Chang, X. Jiang, S. Hua, C. Yang, J. Wen, L. Jiang, G. Li, G. Wang, and M. Xiao, Nat. Photonics **8**, 524 (2014).
[19] M. Brandstetter, M. Liertzer, C. Deutsch, P. Klang, J. Schöberl, H. E. Türeci, G. Strasser, K. Unterrainer, and S. Rotter, Nat. Commun. **5**, 4034 (2014).
[20] H. Hodaei, M.-A. Miri, M. Heinrich, D. N. Christodoulides, and M. Khajavikhan, Science **346**, 975 (2014).
[21] A. Regensburger, C. Bersch, M.-A. Miri, G. Onishchukov, D. N. Christodoulides, and U. Peschel, Nature **488**, 167 (2012).
[22] L. Feng, Y.-L. Xu, W. S. Fegadolli, M.-H. Lu, J. E. B. Oliveira, V. R. Almeida, Y.-F. Chen, and A. Scherer, Nat. Mater. **12**, 108 (2013).
[23] L. Feng, Z. J. Wong, R.-M. Ma, Y. Wang, and X. Zhang, Science **346**, 972 (2014).
[24] S. Sandhu, M. L. Povinelli, and S. Fan, Opt. Lett. **32**, 3333 (2007).
[25] K. Ding, Z. Q. Zhang, and C. T. Chan, Phys. Rev. B **92**, 235310 (2015).
[26] L. Ge, Phys. Rev. A **92**, 052103 (2015).
[27] A. Szameit, M. C. Rechtsman, O. Bahat-Treidel, and M. Segev, Phys. Rev. A **84**, 021806 (2011).
[28] H. Ramezani, T. Kottos, V. Kovanis, and D. N. Christodoulides, Phys. Rev. A **85**, 013818 (2012).
[29] B. Zhen, C. W. Hsu, Y. Igarashi, L. Lu, I. Kaminer, A. Pick, S.-L. Chua, J. D. Joannopoulos, and M. Soljačić, Nature **525**, 354 (2015).
[30] L. Ge and A. D. Stone, Phys. Rev. X **4**, 031011 (2014).
[31] J. Joannopoulos, S. Johnson, J. Winn, and R. Meade, *Photonic Crystals: Molding the Flow of Light (Second Edition)*.
[32] H. Kosaka, T. Kawashima, A. Tomita, M. Notomi, T. Tamamura, T. Sato, and S. Kawakami, Phys. Rev. B **58**, R10096 (1998).
[33] H. Kosaka, T. Kawashima, A. Tomita, M. Notomi, T. Tamamura, T. Sato, and S. Kawakami, J. Lightwave Technol. **17**, 2032 (1999).
[34] C. Luo, S. G. Johnson, J. D. Joannopoulos, and J. B. Pendry, Phys. Rev. B **65**, 201104 (2002).
[35] X. F. Yu and S. H. Fan, Appl. Phys. Lett. **83**, 3251 (2003).
[36] A. Yariv, Y. Xu, R. K. Lee, and A. Scherer, Opt. Lett. **24**, 711 (1999).
[37] M. Soljačić, S. G. Johnson, S. Fan, M. Ibanescu, E. Ippen, and J. D. Joannopoulos, J. Opt. Soc. Am. B **19**, 2052 (2002).
[38] See supplementary material.
[39] N. Johnson and P. Hui, J. Phys.-Condens. Mat. **5**, L355 (1993).
[40] N. F. Johnson, P. M. Hui, and K. H. Luk, Solid State Commun. **90**, 229 (1994).
[41] P. B. Allen, T. Berlijn, D. A. Casavant, and J. M. Soler, Phys. Rev. B **87**, 085322 (2013).
[42] J. E. Sipe, Phys. Rev. E **62**, 5672 (2000).
[43] V. Liu and S. Fan, Computer Physics Communications **183**, 2233 (2012).
[44] W. Shin and S. Fan, Journal of Computational Physics **231**, 3406 (2012).